Science Translational Medicine
AAAS

Microfluidic CD4+ and CD8+ T Lymphocyte Counters for Point-of-Care HIV Diagnostics Using Whole Blood

Nicholas N. Watkins *et al.*

Sci Transl Med **5**, 214ra170 (2013);
DOI: 10.1126/scitranslmed.3006870

Editor's Summary

Tiny T Cell Counter for HIV

The amount of CD4 and CD8 T cells in a blood sample can tell a doctor the status of the patient's immune system and HIV infection. Current methods of counting aren't always available in resource-poor settings, such as Sub-Saharan Africa, so Watkins *et al.* created a microfluidic chip for these point-of-care (POC) settings, which incorporates all steps of sample preparation and accurate T cell counting.

The microfluidic differential T cell counter is based on the Coulter counter principle: In the device, cells are flowed through a tiny pore that has a current passing through it; the cell, which doesn't conduct electricity, then blocks the current and causes a "spike" in signal. The number of spikes told Watkins *et al.* how many cells traveled through the pore. The device also integrated sample preparation and cell selection. Red blood cells were lysed and removed from the sample, leaving primarily white blood cells (including T cells). Antibodies decorated the microfluidic channels, to capture the population of choice —either CD4 or CD8 T cells. Thus, by obtaining a total cell count at the beginning and a final count at the end, the authors were able to quantify the number of T cells in the sample. Blood samples from HIV-infected donors and healthy volunteers were tested and compared to the gold standard, flow cytometry. Watkins and colleagues found that their differential T cell counter worked as well as flow cytometry in counting $CD4^+$ and $CD8^+$ T cells, thus suggesting that it is a viable platform for tracking HIV infection.

Unique to this device is the ability to monitor not only CD4 cells but also CD8 T cells, which can give a more complete picture of infection. By integrating all steps of POC detection —sample preparation, purification, and analysis —and costing less per test than certain flow cytometers, it is possible that this device will be useful in resource-limited settings. Nevertheless, more testing on patients over time will be necessary to determine the device's clinical utility.

Science Translational Medicine (print ISSN 1946-6234; online ISSN 1946-6242) is published weekly, except the last week in December, by the American Association for the Advancement of Science, 1200 New York Avenue NW, Washington, DC 20005.

HIV DIAGNOSTICS

Microfluidic CD4$^+$ and CD8$^+$ T Lymphocyte Counters for Point-of-Care HIV Diagnostics Using Whole Blood

Nicholas N. Watkins,[1,2*†] Umer Hassan,[1,2*] Gregory Damhorst,[2,3] HengKan Ni,[1,2] Awais Vaid,[4] William Rodriguez,[5] Rashid Bashir[2,3‡]

Roughly 33 million people worldwide are infected with HIV; disease burden is highest in resource-limited settings. One important diagnostic in HIV disease management is the absolute count of lymphocytes expressing the CD4$^+$ and CD8$^+$ receptors. The current diagnostic instruments and procedures require expensive equipment and trained technicians. In response, we have developed microfluidic biochips that count CD4$^+$ and CD8$^+$ lymphocytes in whole blood samples, without the need for off-chip sample preparation. The device is based on differential electrical counting and relies on five on-chip modules that, in sequence, chemically lyses erythrocytes, quenches lysis to preserve leukocytes, enumerates cells electrically, depletes the target cells (CD4 or CD8) with antibodies, and enumerates the remaining cells electrically. We demonstrate application of this chip using blood from healthy and HIV-infected subjects. Erythrocyte lysis and quenching durations were optimized to create pure leukocyte populations in less than 1 min. Target cell depletion was accomplished through shear stress–based immunocapture, using antibody-coated microposts to increase the contact surface area and enhance depletion efficiency. With the differential electrical counting method, device-based CD4$^+$ and CD8$^+$ T cell counts closely matched control counts obtained from flow cytometry, over a dynamic range of 40 to 1000 cells/μl. By providing accurate cell counts in less than 20 min, from samples obtained from one drop of whole blood, this approach has the potential to be realized as a handheld, battery-powered instrument that would deliver simple HIV diagnostics to patients anywhere in the world, regardless of geography or socioeconomic status.

INTRODUCTION

The CD4$^+$ T cell count is a critical test in the management of HIV/AIDS and is widely used to determine when to initiate antiretroviral therapy and to monitor the efficacy of treatment. Of the 33 million people living with HIV globally, 7.5 million are eligible for treatment but may not be aware of their CD4$^+$ count (*1*). The CD4$^+$ count is usually expressed as the absolute number of CD4$^+$ T lymphocytes per microliter of blood. In addition, the ratio of CD4$^+$ cells to the total lymphocyte count (the CD4 percentage) and the ratio of CD4$^+$ T cells to CD8$^+$ T cells (CD4/CD8) are particularly useful in monitoring the course of infection and give an overall assessment of the body's immune strength. The CD4/CD8 ratio is also especially useful for HIV-infected infants, because there is a marked increase in CD8 T cells while the depletion of CD4 T cells due to HIV infection is not apparent in their early life (*2*–*5*). Flow cytometry is the standard diagnostic method for CD4 counting, but it requires centralized laboratory facilities and trained personnel—neither of which are routinely available in poverty-stricken regions with limited resources. As a result, much effort has been placed in creating portable and inexpensive CD4$^+$ T cell counters that would bring CD4 counts to the point of care (POC), eliminating socioeconomic or geographic barriers that currently prevent access to 69% of HIV-infected people in resource-limited settings like Sub-Saharan Africa (*1*).

Many of the first-generation POC CD4$^+$ cell counting methods rely on microfluidic adaptations of flow cytometry, such as microfluidic image cytometers, which obtain counts by analyzing images of fluorescently labeled CD4$^+$ T cells (*6*–*9*), or miniaturized flow cytometry platforms (*10*–*12*) that may still require manual processing and blood volumes larger than a finger stick. More portable methods, such as immunochromatographic strips that compare labeled CD4$^+$ cells to a reference strip (*13*), or a recently described sedimentation system that provides CD4 counts based on the height of CD4-conjugated beads in a viewing window (*13*, *14*), may not always provide sufficient accuracy to monitor progression of therapy. Novel approaches using scanning fluorescence microscopy and quantum dots or fluorescence-labeled antibodies (*15*) generally require off-chip sample processing and manual handling steps (*3*).

Owing to simplicity and low cost, electrical detection methods hold much promise for POC cytometry. Much progress has been made in impedance microcytometry with alternating current interrogation to detect differences in chemically modified cells (*16*–*18*) and cells infected with parasites (*17*), and to discriminate among cell types (*19*–*22*). Nevertheless, impedance microcytometry still has not proven to be sensitive enough to distinguish among cells that have similar morphologies, such as lymphocyte subclasses and monocytes. Microparticle impedance labels have been shown to alter the high-frequency signature of CD4$^+$ T cells enough to distinguish them from other lymphocytes, but require off-chip bead labeling steps (*23*). A technique that can be used at the POC, which provides single-cell counting accuracy for multiple cell subtypes and eliminates any manual steps, has not, to our knowledge, been reported.

As one initial approach, we previously described a method for counting cells based on differential measurements of cell counts using

[1]Department of Electrical and Computer Engineering, University of Illinois at Urbana-Champaign, William L. Everett Laboratory, 1406 West Green Street, Urbana, IL 61801, USA. [2]Micro and Nanotechnology Laboratory, University of Illinois at Urbana-Champaign, 208 North Wright Street, Urbana, IL 61801, USA. [3]Department of Bioengineering, University of Illinois at Urbana-Champaign, 1270 Digital Computer Laboratory, 1304 West Springfield Avenue, Urbana, IL 61801, USA. [4]Champaign Urbana Public Health District, 201 West Kenyon Road, Champaign, IL 61820, USA. [5]Daktari Diagnostics Inc., 85 Bolton Street, Cambridge, MA 02140, USA.
*These authors contributed equally to this work.
†Present address: Nabsys Inc., 60 Clifford Street, Providence, RI 02903, USA.
‡Corresponding author. E-mail: rbashir@illinois.edu

electrical impedance (*24*). The cell counting is based on the Coulter counting principle (*25*). A cell is a nonconducting particle that will block the electrical current being passed through a microfluidic pore. The cell passage through the pore will create a spike in impedance having an amplitude and width proportional to the size of the cell and the cell's translocation velocity through the pore, respectively. This technique is used not only to obtain cell concentration but also to distinguish between different cell types in heterogeneous cell populations on the basis of their size and morphology, using a variety of applied bias frequencies (*26*). A microfabricated electrical cytometer based on the Coulter principle could provide accurate CD4 counts by counting cells individually. Such a system would have the advantages of electrical CD4 cell counting methods, with accuracy that should be higher than bulk electrical impedance methods described by our group and others (*27*).

Here, we report an integrated microfluidic differential counter design that incorporates on-chip sample preparation to provide accurate $CD4^+$ or $CD8^+$ T cell counts from 10 μl of undiluted, unprocessed human blood samples. From these counts, CD4/CD8 ratios were also obtained, which correlated well with control counts from a hospital's flow cytometry facility for both healthy and HIV-infected blood samples. The lack of optics allows for a streamlined design that can be

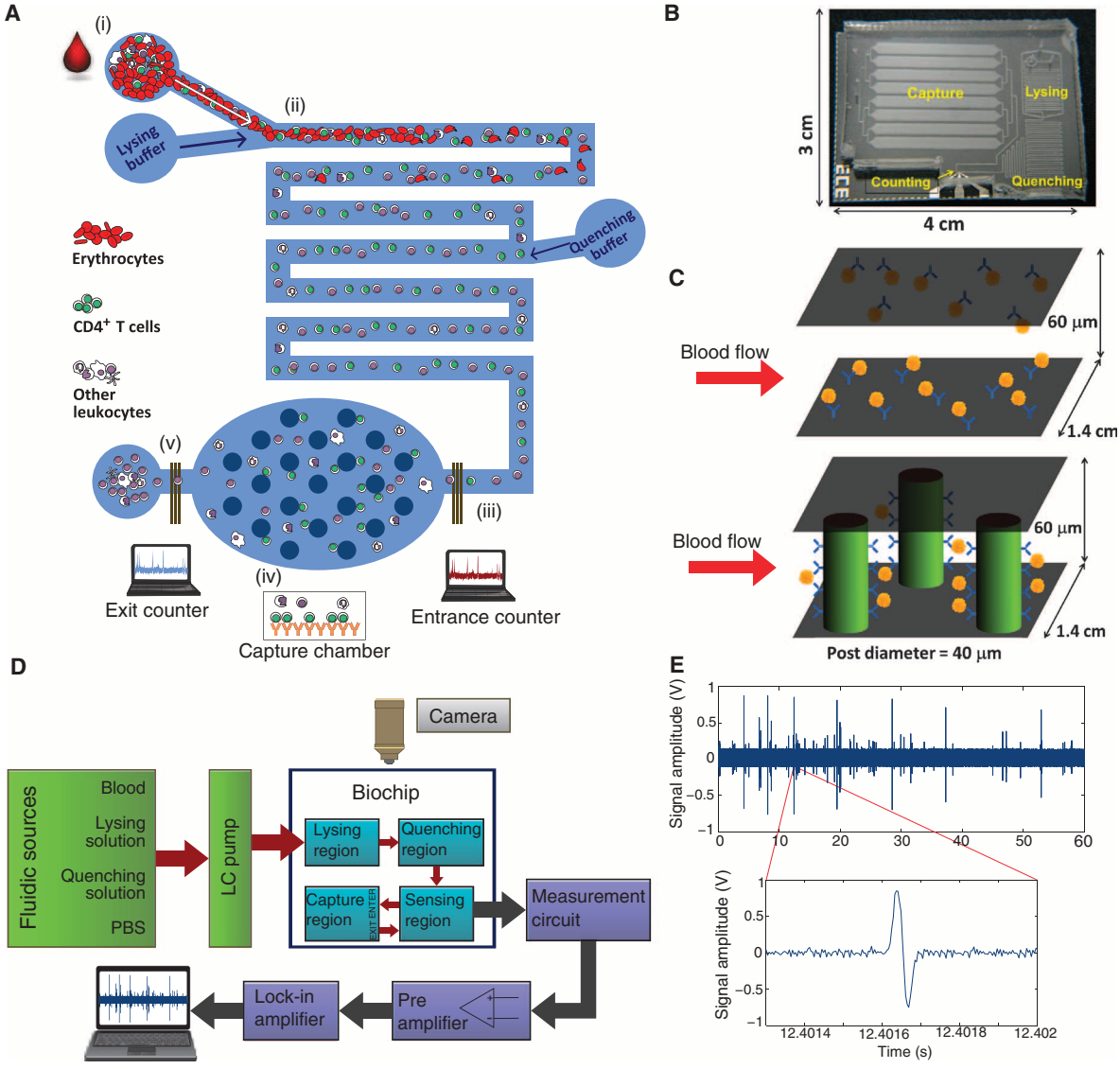

Fig. 1. Principle of counting $CD4^+/CD8^+$ T cells from whole blood samples. (**A**) Graphical schematic of the microfluidic chip design and sample processing. (i) Infusion of 10 μl of blood in the chip using a liquid chromatography (LC) pump. (ii) On-chip erythrocyte lysis. (iii) The entrance counter gives the total counts of all leukocytes. (iv) The capture chamber immobilized with CD4 or CD8 antibodies capture $CD4^+$ or $CD8^+$ T cells, respectively. (v) Exit counter counts the remaining cells. The difference in counts gives the number of captured T cells. (**B**) Image of the fabricated chip with a planar capture chamber and entrance counter. (**C**) Two device designs explored in this study. The antibody is attached to the surface in the planar capture chamber (top). Antibody is attached to posts in the capture chamber (bottom). (**D**) Graphical layout of the experimental and measurement setup. (**E**) Typical bipolar pulses obtained as the cells pass through the electrodes. Inset shows the zoomed-in region of the signal.

realized as a battery-powered, handheld unit that analyzes finger prick blood samples via one-time-use, disposable biochips.

RESULTS

Chip design and fabrication

Microfabrication methods were used to create a multilayer fluidic network in polydimethylsiloxane (PDMS) (fig. S1) to enable accurate spatiotemporal control of the injected blood cells and high-resolution electrical impedance sensing, all confined to a small chip footprint of 3 cm × 4 cm (Fig. 1, A and B). In the differential impedance cytometry approach, erythrocyte lysis is necessary to ensure accurate $CD4^+$ T cell counts, as the sheer number of erythrocytes (~2000-fold greater than leukocyte concentrations) would require large sample dilutions, thus increasing analysis time and the probability of counting error. Figure 1A shows a schematic of integrated electrical differential counting approach. The lysis module selectively ruptures the membranes of erythrocytes over several seconds through diffusive mixing of a lysis solution of saponin and formic acid with the focused blood stream (*22*). The quenching region introduces a buffer to halt lysis, preserving the leukocytes in a debris-free solution that is subsequently processed using the differential electrical counting principle (*24*).

The 300-fl sense volume in the counting channel (15 μm tall × 15 μm wide) ensured sufficient signal-to-noise event detection and reduced the possibility of multiple cells being counted simultaneously as compared to the case when the sense volume is much larger than the cell volume. The sense volume was about four orders of magnitude less than the average volume per leukocyte found in patients with abnormally high leukocyte counts (>12,000 cells/μl). We explored both a planar capture chamber design and a design modified to include posts, to increase surface area, and to improve the cell capture efficiency (Fig. 1C). Figure 1D shows the experimental setup for flowing the fluid during the measurement. The three coplanar electrodes generated bipolar pulses due to the passage of each cell (Fig. 1E). A dual-frequency (303 kHz and 1.7 MHz) electrical interrogation method was used to obtain information about the leukocyte population by observing the cell membrane capacitance in addition to their size (*26*).

Erythrocyte lysis and quenching optimization

The blood sample was focused by lysis buffer sheaths (Fig. 2A). Erythrocytes were ruptured as they flowed through serpentine mixing channels (Fig. 2, A and B, and movie S1). After completing the lysing and quenching processes, the recovered leukocytes could be seen flowing through the device (Fig. 2C). The recovered cells were collected and tagged with CD45 fluorescent antibody, and the sample was run through a flow cytometer to confirm the presence of leukocytes. The optimal erythrocyte lysis duration is crucial because it needs to be long enough to rupture all the erythrocyte membranes, but short enough to preserve the remaining leukocytes. This window was found by locking the flow ratio between blood and lysis solution at 1:12 (v/v) and varying the total flow rate to give different resident times in the lysing region before lysis was halted in the quenching region.

Figure 2D illustrates how on-chip lysis duration affected the population distribution of the leukocytes. Each scatter plot compares the low-frequency (303 kHz) impedance magnitude, $|Z|$, to the opacity—the ratio of the high-frequency impedance at 1.7 MHz to the low-frequency impedance—for a particular lysis time. [The low-frequency impedance level is proportional to the size of the cell, whereas the electrical opacity gives information about the cell's membrane, independent of cell size (*26*, *28*, *29*).] As lysis time increased, a portion of the granulocyte/monocyte population transitioned from its original population (at 2 s—the optimal lysis time) to between the lymphocyte and granulocyte/monocyte populations (at 6 s) to its final position, which partially overlaps the smaller-sized portion of the lymphocyte population (at 8 to 10 s). Eventually, membranes became fully permeabilized, forming the third population of cells at 10 s (Fig. 2D). At 303 kHz, the permeabilized cells cannot be represented as nonconducting particles anymore, as electrical conduction takes place through the cell, resulting in smaller impedance at 303 kHz (a 64% decrease between the granulocytes/monocyte population and the permeabilized population at 10 s). The

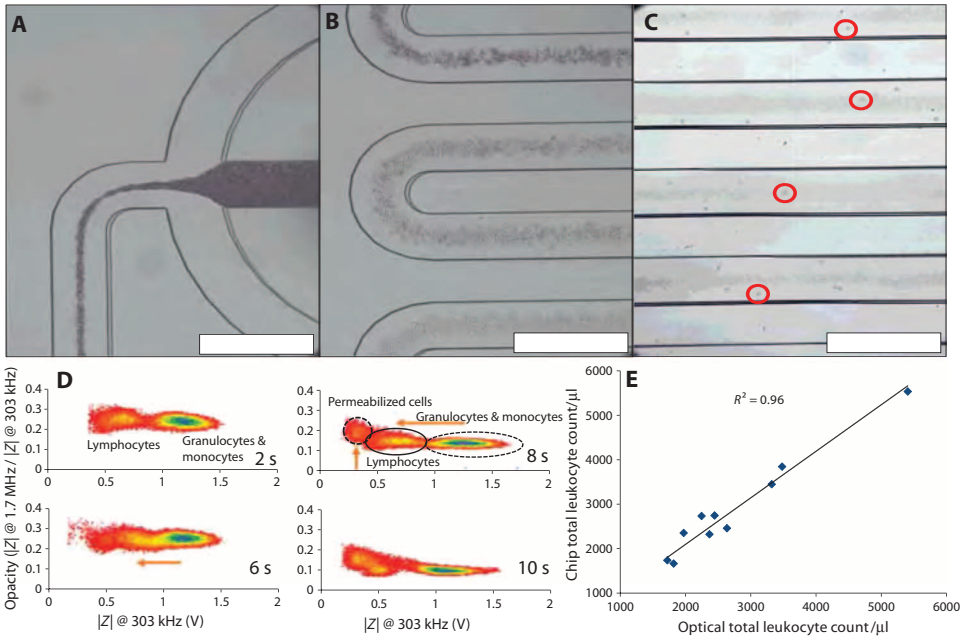

Fig. 2. Effects of lysis time on erythrocytes and leukocytes. Real-time videos of these processes are in movie S1. (**A**) Focusing of the blood sample by lysis buffer sheaths. (**B**) Rupturing of erythrocytes as they flow through the serpentine mixing channels. (**C**) Leukocytes recovered after quenching the lysis process. Four of the eighteen leukocytes seen in this panel are encircled (in red). Scale bars, 400 μm (A to C). (**D**) Effects of lysis time on leukocytes. Low-frequency impedance (303 kHz) versus opacity ($|Z|$ at 1.7 MHz/$|Z|$ at 303 kHz) scatter plots showing the effect of lysing duration on the granulocyte/monocyte population. The arrows illustrate the movement of the permeabilized population as the lysis duration increases from 2 to 10 s. (**E**) Electrical chip leukocyte counts versus the optical counts obtained from a Guava EasyCyte Plus flow cytometer in our laboratory (n = 10 samples), with the solid line representing the best linear fit.

1.7-MHz impedance also decreased (42%) for similar reasons, but not to the same extent as at 303 kHz—which explains the 63% increase in the permeabilized population's opacity as the high-frequency impedance would already be electrically interrogating the unpermeabilized cells' interiors. To ensure the accuracy of the electrical counting procedure, we compared the electrical counts with the counts from the flow cytometer (Fig. 2E). We calculated an R^2 value of 0.96, validating the electrical counting measurement procedure.

An optimal quenching solution composed of concentrated phosphate-buffered saline (PBS) and sodium bicarbonate kept the counting error at 3% (n = 20) (fig. S2). Experiments were also performed to find the minimum quench duration needed to create a debris-free leukocyte solution. Quenching times of 7.5 and 11.3 s did not allow the saponin to completely disassociate the erythrocyte fragments or "ghosts" that were created from the exposure to formic acid (Fig. 3A) (*27*). These fragments still create an appreciable change in impedance when they pass through the counter, resulting in a baseline noise level that masks many leukocytes. The low-frequency impedance pulse histograms in Fig. 3A show that the erythrocyte debris dominated all counts at 7.5 and 11.3 s. Complete erythrocyte lysis and debris removal occurred between 11.3 and 15.4 s, as the pulse signal-to-noise ratio of about 21.8 was similar to that found by analyzing leukocyte populations that were prepared using off-chip techniques, which includes lysing, quenching, and washing twice via centrifuge. In addition, the baseline root-mean-square (RMS) noise of 28 mV at 15.4 s was similar to that found for the 48.3 s quench duration (Fig. 3A). However, the erythrocyte debris peak at 15.4 s was completely removed at 48.3 s, which was confirmed visually by micrographs (Fig. 3B); therefore, the minimum quenching

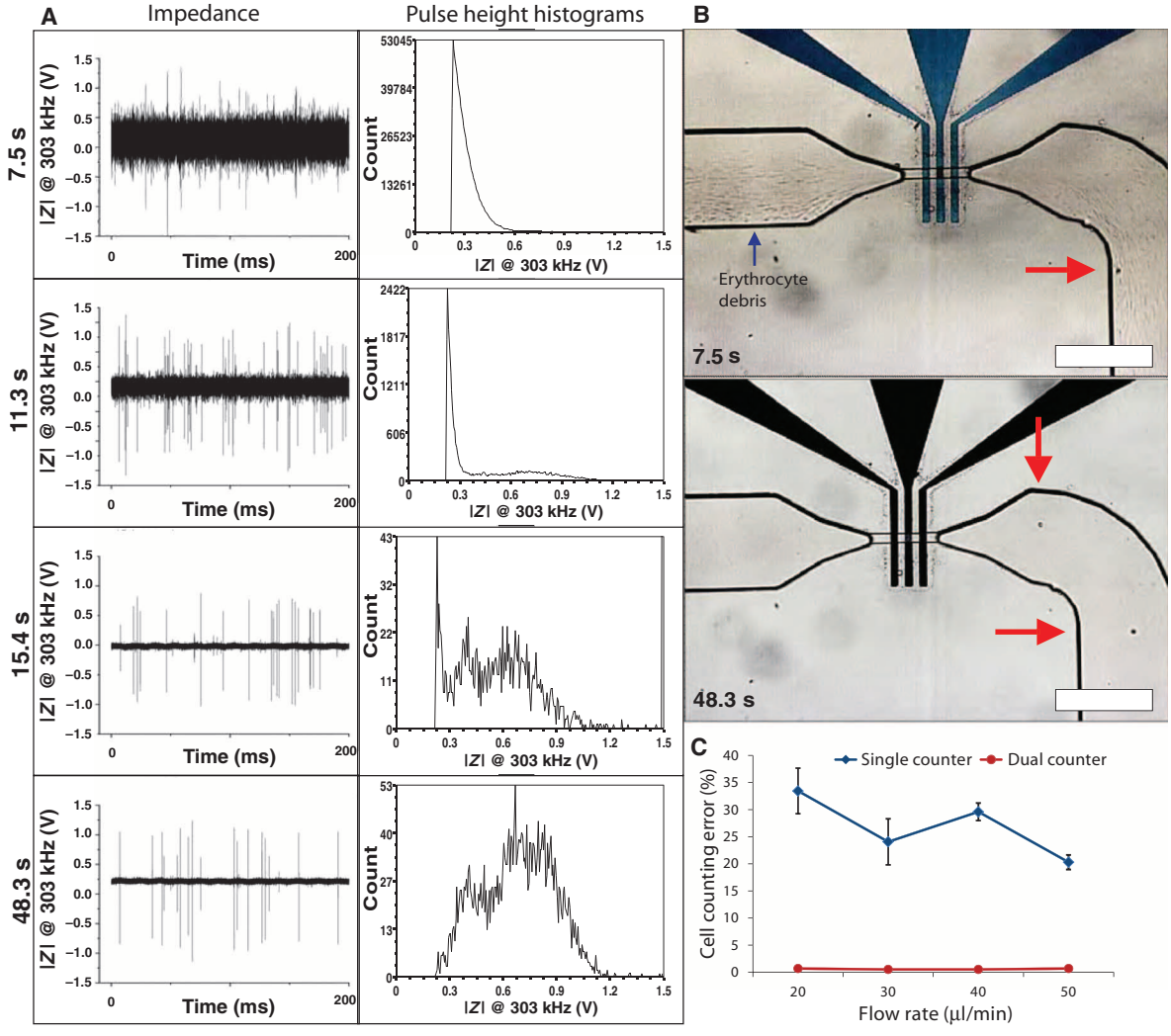

Fig. 3. Effects of quenching time on erythrocyte debris. (**A**). Impedance signals and resultant pulse height histograms for various quenching times of whole blood samples. Histograms were created by analyzing impedance data using a threshold level of 0.22 V. The impedance plots are 200-ms snapshots of the electrical data analyzed to create their respective histograms. Impedance pulse plots were plotted at the same scale for pulse height and baseline noise comparison. (**B**) Micrographs of the counting channel at different quenching times of whole blood samples. Erythrocyte debris is noticeable at 7.5 s and is absent at 48.3 s. Flow direction is from left to right in all micrographs. Arrows signify the position of leukocytes along the channel. Scale bars, 200 µm. (**C**) Comparison of cell counting error between the forward/reverse flow technique (single counter) with forward flow (dual counter). Data are averages ± SD (n = 3 experiments).

time should be about 48 s to ensure that all erythrocyte debris is removed, ensuring adequate separation from the electrical noise and that no debris is falsely counted as leukocytes.

We also investigated the effects of lysing and quenching reagents on cell viability. For a single counter case, the flow is reversed for the exit count and cells were exposed to reagents for varying times depending on flow rate (table S1). We observed a difference of almost 20% cell loss between forward and reverse counts. However, when two counters were used—one at the entrance and another at the exit of the capture chamber—exposure to the reagents was reduced to less than 1 min (table S1), which resulted in <1% cell loss (Fig. 3C).

$CD4^+/CD8^+$ T lymphocyte capture

We next calculated the efficiency of capture of $CD4^+$ (or $CD8^+$ T) lymphocytes using a chamber coated with CD4 (or CD8) antibodies (fig. S3). Whole-blood samples (10 μl) from healthy volunteers were analyzed on-chip at varying capture chamber shear stresses to find the optimal shear stress that would provide the highest capture efficiency, resulting in the most accurate representative $CD4^+$ or $CD8^+$ T cell count. For a planar capture chamber, the maximum capture efficiency of 44.5% was obtained at 0.088 dyn/cm^2 (fig. S4). At this shear stress, the cells have ample interaction time with the immobilized antibodies on the chamber floor. By contrast, at 0.333 dyn/cm^2, the capture efficiency markedly decreased.

Adding pillars in the capture chamber could result in a higher capture efficiency by increasing antibody-cell interactions via larger chamber surface area. Four different designs with varying spacing of 8, 11, 14, and 17 μm between posts were explored. We found that the 11-μm post spacing provided small enough spacing to give the ~8-μm-diameter lymphocyte contact with the antibody-coated pillar surfaces, but large enough to prevent larger leukocytes from clogging the pathways (Fig. 4A). With a capture chamber footprint of 2.5 cm × 1.4 cm and 40-μm-diameter posts with 11-μm spacing, the total number of posts in the capture chamber was about 134,000. On-chip lysed and quenched blood samples were injected into the capture chamber (Fig. 4C) at flow rates ranging from 15 to 30 μl/min to find the optimal shear stress for maximum capture efficiency. This capture chamber design was simulated in COMSOL to get the corresponding shear stress values at the surface of the pillars for the different flow rates (fig. S5). Two-dimensional (2D) simulation for a flow rate of 20 μl/min resulted in a maximum shear stress of 0.11 dyn/cm^2 at the pillar walls (Fig. 4B) with maximum capture efficiencies of 98.3 and 90.1% for $CD4^+$ T cells and $CD8^+$ T cells, respectively (Fig. 4C) (movies S2 and S3).

The capture of different cells in the capture chamber was investigated for both CD4 and CD8 T cell capture experiments (Fig. 4D). Ten percent of lymphocytes other than $CD4^+$ T cells and 52% of granulocytes/

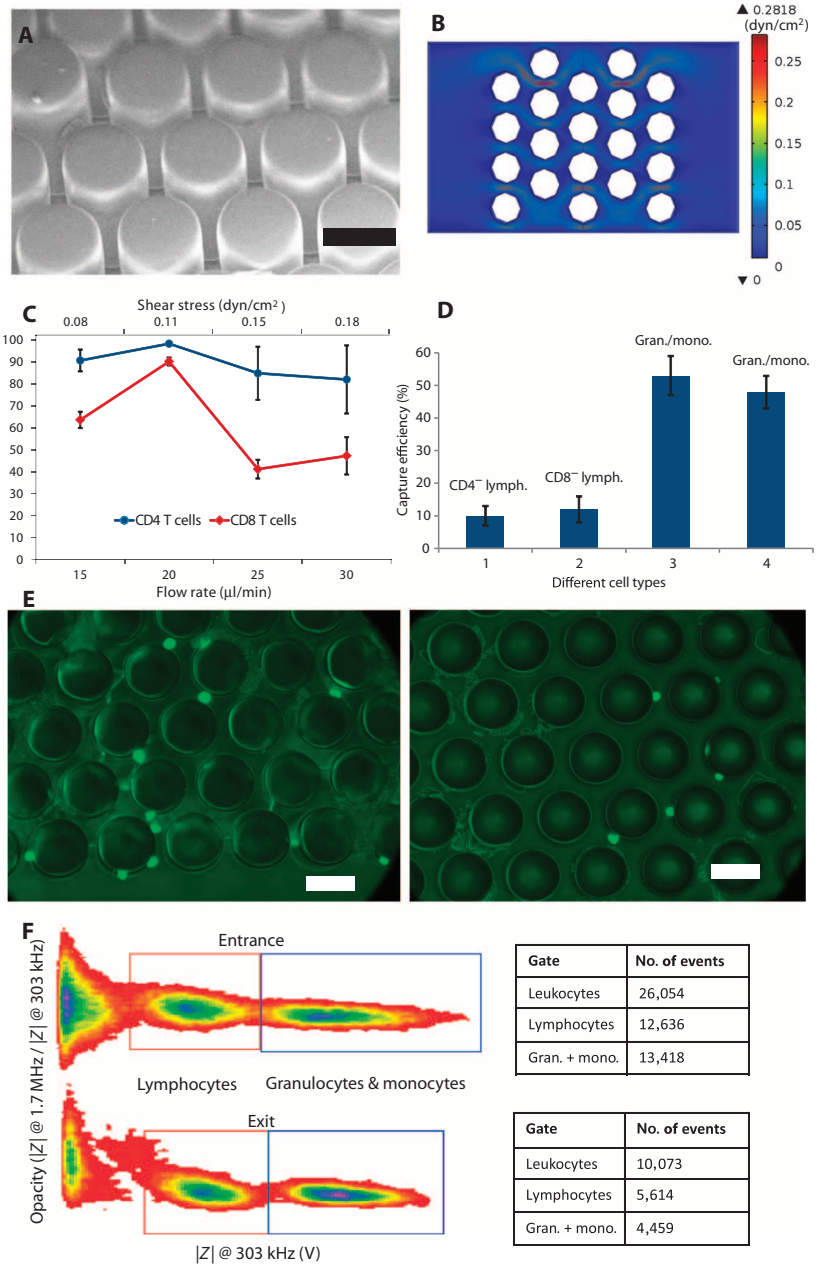

Gate	No. of events
Leukocytes	26,054
Lymphocytes	12,636
Gran. + mono.	13,418

Gate	No. of events
Leukocytes	10,073
Lymphocytes	5,614
Gran. + mono.	4,459

Fig. 4. Pillars in the capture chamber result in high capture efficiency. (**A**) Scanning electron microscopy image of the posts with a height of 60 μm and a diameter of 40 μm. The spacing between the posts is 11 μm. Scale bar, 40 μm. (**B**) 2D shear stress simulation at 20 μl/min in COMSOL. (**C**) Capture efficiency at different flow rates (shear stresses) for $CD4^+$ and $CD8^+$ T cells. Data are means ± SD (n = 4). (**D**) Capture efficiencies of different cell types. (1) Lymphocytes other than $CD4^+$ T cells captured by CD4 antibodies. (2) Lymphocytes other than $CD8^+$ T cells captured by CD8 antibodies. (3) Granulocytes/monocytes captured by CD4 antibodies. (4) Granulocytes/monocytes captured by CD8 antibodies. Data are means ± SD (n = 3). Within one experiment, the percent capture of different cell types is shown in fig.S6. (**E**) (Left) False-colored fluorescent image of $CD4^+$ T cells (green) captured in between posts in an anti-CD4 capture chamber. (Right) False-colored fluorescent image of $CD8^+$ T cells (green) captured in between posts in an anti-CD8 capture chamber. Scale bars, 40 μm. (**F**) $CD4^+/CD8^+$ T cell counting method. Opacity versus low-frequency impedance scatter plots of a $CD4^+$ T lymphocyte capture experiment. A gating technique (rectangular boxes selected to include leukocytes) was used to determine the total leukocyte (sum of lymphocyte and granulocyte/monocyte count) and lymphocyte counts for both entrance and exit counters. Populations outside the boxes are debris.

monocytes were captured in a CD4 capture experiment. Twelve percent of lymphocytes other than $CD8^+$ T cells and 48% of monocytes/granulocytes were captured in a CD8 capture experiment. The capture purity—or percentage makeup of different captured cell types—when anti-CD4 or anti-CD8 antibody was adsorbed in the capture chamber is shown in fig. S6. It was found that, among captured cells, 43% were $CD4^+$ and 42% were $CD8^+$ T cells in their respective capture experiments. To verify the capture of the $CD4^+$ or $CD8^+$ T cells, the cells in the capture chamber were labeled with fluorescent CD4 and CD14 antibodies (CD14 can be used to differentiate monocytes) or CD8 antibodies. The cells were further stained with 4′,6-diamidino-2-phenylindole for leukocyte determination and fixed with paraformaldehyde. Fluorescently labeled $CD4^+$ and $CD8^+$ T cells were then imaged in separate capture chambers to optically verify the cell capture (Fig. 4E).

Figure 4F shows the scatter plots of low-frequency impedance versus opacity for a $CD4^+$ T lymphocyte capture experiment. A gating technique—a region on a scatter plot to include all leukocytes, lymphocytes, and/or granulocytes/monocytes—similar to flow cytometry was used to determine the total lymphocyte counts for both entrance and exit counters (Fig. 4F). The difference in counts obtained at the entrance and exit reflected the number of cells captured in the capture chamber.

$CD4^+/CD8^+$ T cell count comparison to flow cytometry

Blood samples from 18 healthy volunteers and 32 HIV-infected patients undergoing antiretroviral therapy were analyzed for $CD4^+$ and $CD8^+$ T cell counts using our electrical differential counting technique with on-chip sample preparation. Electrical differential counting was compared to flow cytometry for $CD4^+$ and $CD8^+$ T cells and for the CD4/CD8 ratio from healthy volunteers (Fig. 5) and HIV-infected subjects (Fig. 6). Hematocrit was also plotted along with the cell counts, which showed no correlation between hematocrit level and flow cytometer cell count (fig. S7). Bland-Altman analyses showed good agreement between the two counting methods over the entire $CD4^+/CD8^+$ T cell counting range for healthy samples (table S2). A positive bias of almost 24 cells/μl showed that, on average, the biochip gave slightly higher CD4 counts than the hospital's flow cytometer (Fig. 5A). CD8 counts resulted in a positive bias of 9 cells/μl, showing even better accuracy (Fig. 5B). A negligible bias of 0.012 existed for the CD4/CD8 ratio (Fig. 5C).

The microchip's counting accuracy was quantified by finding the absolute average percent error (difference normalized by flow cytometry count) between the two methods. The error was found to be 2.9% for CD4, 1.6% for CD8, and 1.9% for the CD4/CD8 ratio. Both counting methods were also compared by Pearson analysis for CD4 and CD8 cells (Table 1). The repeatability of the CD4 and CD8 T cell count from the same blood sample was also performed on healthy blood samples (fig. S8). For the same blood sample, five repeats were performed for both CD4 and CD8, and the coefficient of variation (CV) values were found to be 4.7 and 4.5%, respectively. Variation analysis for a CD4 count of a second sample ($n = 4$) and a CD8 count for a third sample ($n = 3$) resulted in CV values of 2.1 and 1.4%, respectively.

Figure 6 shows the $CD4^+$ T cell count, $CD8^+$ T cell count, and the CD4/CD8 ratio for HIV-infected blood samples. Similar to healthy samples, hematocrit (%) shows no correlation between hematocrit level and any variability in the cell count. A positive bias of 12 cells/μl shows that, on average, the chip gave higher $CD4^+$ T cell counts than the flow cytometer (Fig. 6A). However, the CD8 counts resulted in a negative bias of 55 cells/μl (Fig. 6B). The chip counting error was found to be 5.3% for CD4, 7.4% for CD8, and 11.9% for the CD4/CD8 ratio. Both counting methods were also compared by Pearson analysis for both CD4 and CD8 cells, and the results are shown in Table 1. The

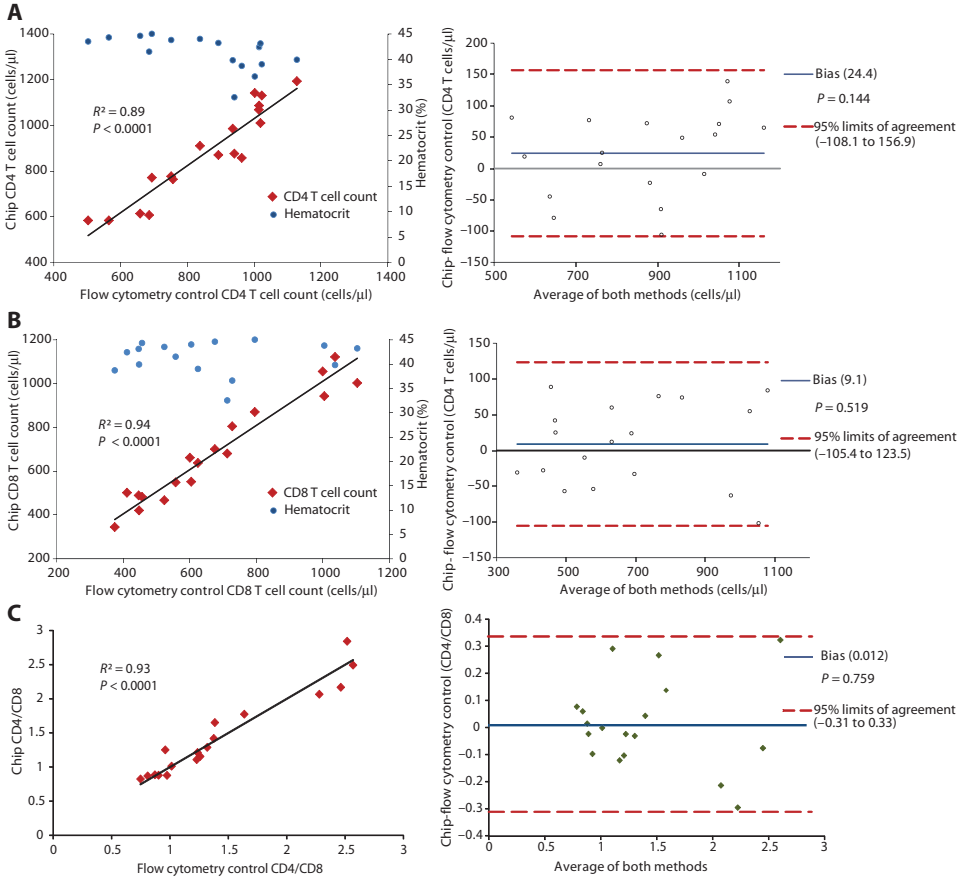

Fig. 5. $CD4^+$ and $CD8^+$ T cell count comparison between chip and flow cytometer control using healthy blood samples. (**A**) $CD4^+$ T cell comparison. (**B**) $CD8^+$ T cell comparison. (**C**) CD4/CD8 ratio comparison. For scatter plots, data points are individual samples ($n = 18$) and the solid line is a linear fit to data with the y intercept set to 0. Hematocrit (%) is also plotted on the second axis. Bland-Altman plots are provided for each comparison; in these plots, the dashed lines represent the upper and lower levels of agreement (95% confidence), whereas the solid blue line shows a bias. Outliers were removed using a two-tailed T distribution. P values were determined as described in Materials and Methods.

high correlation ($R^2 \geq 0.89$; Figs. 5 and 6) and high repeatability (CV $\leq$ 4.7%; fig. S8) of cell counts from our device compared with the "gold-standard" flow cytometry suggest that this electrical differential counting method with on-chip sample preparation could be a viable technology to provide portable and rapid $CD4^+$ and $CD8^+$ T cell counts for patients in resource-poor regions.

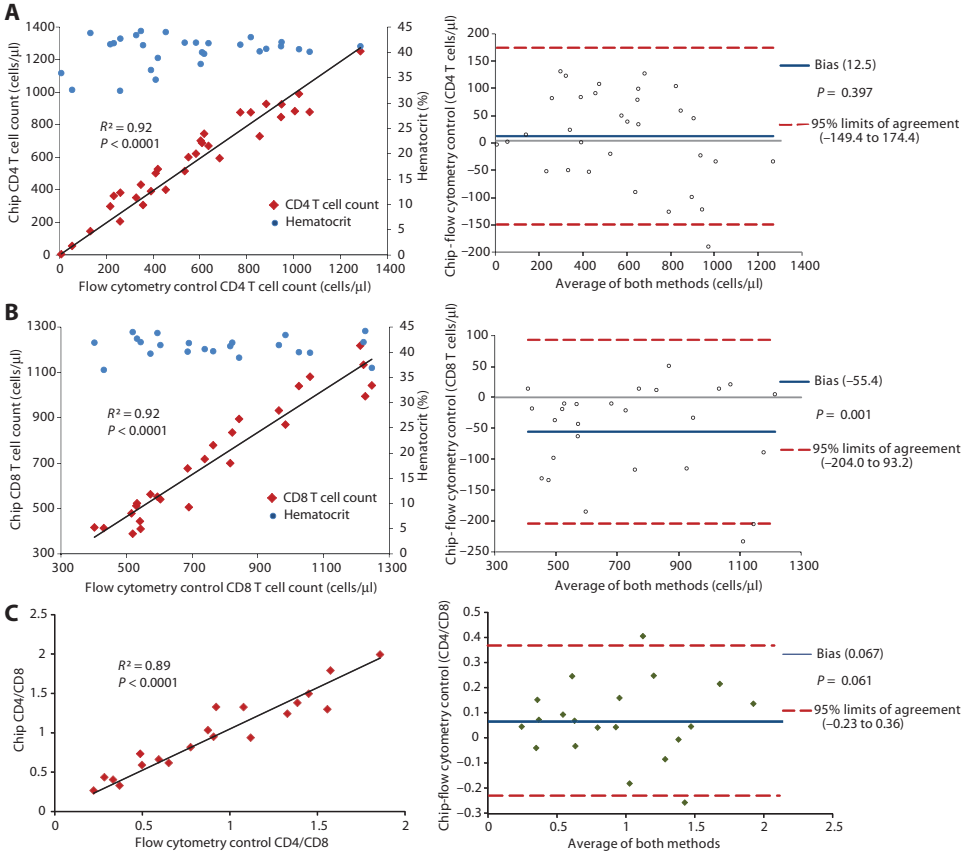

Fig. 6. $CD4^+$ and $CD8^+$ T cell count comparison between chip and flow cytometry control using HIV-infected patient blood samples. (**A**) $CD4^+$ T cell comparison (n = 32). (**B**) $CD8^+$ T cell comparison (n = 26). (**C**) CD4/CD8 ratio comparison from 20 samples for which both $CD4^+$ and $CD8^+$ cells were counted. For scatter plots, data points are individual samples and the solid line is a linear fit to data with the y intercept set to 0. Hematocrit (%) is also plotted on second axis. Bland-Altman plots are provided for each comparison; in these plots, the dashed lines represents the upper and lower levels of agreement (95% confidence), whereas the solid blue line shows a bias. Outliers were removed using a two-tailed T distribution. P values determined as described in Materials and Methods.

DISCUSSION

The on-chip lysing and quenching techniques used in this study proved effective not only in rapidly removing erythrocytes and their debris but also in preserving leukocytes for immunocapture in the capture chamber. An erythrocyte lysis time of only a few seconds ensured that all cells were ruptured for all tested samples, regardless of erythrocyte concentration (3.3 million to 6.0 million cells per microliter of blood). Accordingly, we found no correlation between the accuracy of the chip's measurements and the hematocrit level for all $CD4^+$ and $CD8^+$ T cell counts for both healthy and HIV-infected samples. A slight increase in lysis time may be implemented to ensure accurate CD4 or CD8 counts for patients with elevated erythrocyte counts (>6 million cells/µl). Short-term exposure of leukocytes to saponin during lysis can damage the membranes of some leukocyte subsets (*26*). However, it does not affect cell morphology or membrane antigen expression, which is crucial for our counting technique (*30*). The modified quenching solution quickly brought the leukocytes back to optimal pH and osmotic conditions to preserve them at least for the duration of the experiment.

The dual-frequency electrical interrogation method (*26*) was successful in discriminating lymphocytes from debris and granulocytes/monocytes, allowing for accurate counts simply by obtaining the

Table 1. Comparing chip to flow cytometer. Statistical comparison (R^2 and Pearson) between biochip and flow cytometry control counts from Carle Hospital for $CD4^+$ and $CD8^+$ T lymphocytes collected from healthy and infected donors. A single test ($CD4^+$ and/or $CD8^+$) was performed with each blood sample (except for three samples of which replicates were performed). For 20 HIV-infected subjects, both CD4 and CD8 counts were performed. Further, 12 CD4 and 6 CD8 counting experiments were performed independently from different HIV-infected donors. P values for Bland-Altman (B-A) analysis comparing the chip counts with the flow cytometry control counts.

Sample	Cell count	*n* subjects	R^2	Pearson *r*	Pearson df	*P* value (R^2)	*P* value (B-A)
Healthy	$CD4^+$ T cells	18	0.89	0.94	16	<0.0001	0.144
	$CD8^+$ T cells	18	0.94	0.97	16	<0.0001	0.519
	$CD4^+/CD8^+$	18	0.93	0.96	16	<0.0001	0.759
Infected	$CD4^+$ T cells	32	0.92	0.96	30	<0.0001	0.397
	$CD8^+$ T cells	26	0.92	0.96	24	<0.0001	0.001
	$CD4^+/CD8^+$	20	0.89	0.95	18	<0.0001	0.061

difference between lymphocyte counts before and after exposure to the capture chamber. The low-frequency signal differentiated between lymphocytes (~8 μm in diameter) and the larger granulocytes and monocytes (>10 μm) because a cell's size is directly proportional to its impedance at low frequencies (*31*, *32*). The high-frequency signal was used to further differentiate among the leukocytes and between cells and debris by observing particle capacitance (*18*, *26*, *27*, *29*). For example, monocytes have extensive ruffling and pronounced folds in their membranes that result in an increase in membrane capacitance over similarly sized neutrophils with less prominent ruffles and folds (*33*). However, unlike what Holmes *et al.* demonstrated (*26*), we were not able to distinguish between monocytes and granulocytes, and thus, we grouped them together. It is possible that our coplanar electrode configuration—which is easier to implement than the vertical configuration used by Holmes *et al.*—may prevent us from seeing this slight difference in capacitance (*26*, *29*). A future enhancement would be to improve the current sensing geometry for better leukocyte differentiation and a more comprehensive leukocyte count.

The addition of 11-μm–spaced pillars in the capture chamber improved $CD4^+$ and $CD8^+$ T cell capture efficiency twofold over the planar chamber configuration. The pillars not only increased antibody-antigen interactions via increased chamber surface area but also ensured that the wall shear stress was within the optimal regimen for lymphocyte capture: ~0.1 to 0.3 dyn/cm^2 (fig. S4C). The chip's high capture efficiency and sensitive electrical Coulter counting approach resulted in excellent correlation and accuracy when compared to a clinical flow cytometer—but counting bias did exist. For healthy samples, the positive bias for CD4 and CD8 counts may be attributed to the nonspecific capture of other lymphocytes. The relatively large negative bias obtained for CD8 counts for infected blood samples may be attributed to a lower capture efficiency of the $CD8^+$ T cells as compared to $CD4^+$ T cells, with the mechanism possibly being reduced cell surface receptor expression for infected patients (*34*). The moderately positive bias of $CD4^+$ T cells for infected patients may be from the combination of unwanted lymphocyte capture (positive bias) and poorer capture efficiency due to reduced CD4 receptor expression (negative bias). The positive bias from nonspecific cell capture may be reduced via additional surface chemistry to ensure that surface regions not adsorbed with antibodies are passivated from nonspecific cellular interactions. Slightly decreasing wall shear stress may increase the capture efficiency of lymphocytes that may express less surface receptors in infected patients; however, balance is needed to ensure that the capture of unwanted lymphocytes does not increase significantly for $CD4^+$ and $CD8^+$ T cell counts.

Many have attempted to develop a more portable, automated, and less expensive $CD4^+$ T cell counter (table S3), but few have shown clinical success. The Alere Pima CD4 bench-top system has shown to be the most successful automated next-generation CD4 counter in resource-poor regions, using optical fluorescence detection in single-use, disposable test cartridges that provide $CD4^+$ T cell counts in about 20 min (*9*). In contrast, the device described in this paper uses only electrical methods to interrogate blood samples, thereby eliminating the need for expensive detection optics (that is, light source, lenses, filters, charge-coupled device). The lack of optics and the presence of a self-referencing impedance sensing method in the analysis unit (*24*) would consume less battery power and make it less susceptible to environmental changes, such as temperature, humidity, and mechanical shock or vibration. With further integration, the microfluidic biochips described here would be packaged as a single-use, disposable module that is inserted into a handheld analysis unit, accepts finger prick blood samples, and contains all reagents. Modifying the capture chamber to handle higher flow rates could provide over twice the testing throughput of the Pima CD4. In addition, our device was shown to be at least as accurate as the Pima CD4 system, with a CD4 counting bias of 12 cells/μl, compared to the Pima CD4's bias of −121 cells/μl over similar CD4 T cell concentration ranges in HIV-infected patient samples (table S3) (*9*). For CD4 T cell counts less than 250 cells/μl, our device was comparable, with a bias of 9, compared to the Pima CD4's bias of −10.8 (*9*). The CV of the counter chip for $CD4^+$ T cell counts from healthy samples was 2.1 to 4.7% (two samples, four to five replicates), which is less than the 10.7% CV for the Pima CD4 with patient samples (103 samples, duplicates) (*35*). Our chip has CV values that are considerably less than the accepted standard of 15% for flow cytometry, which would also be a suitable standard for translation to POC.

In conclusion, the microfluidic device described in this study shows potential to accurately count $CD4^+$ and $CD8^+$ T cells from a drop of blood and allow HIV/AIDS diagnostics to penetrate resource-poor regions of the world. In addition to HIV/AIDS, our technology could also be used for individualized cell counting of other cell types in various settings, including at home, in doctors' offices, and at the hospital bedside.

MATERIALS AND METHODS

Study design

To achieve a <5% SEM for the microfluidic CD4/CD8 T cell counts when compared to the flow cytometer's counts, and assuming an SD of 200 cells/μl for healthy donors (typical value of 1000 cells/μl), a minimum of 16 samples would be needed. This is found by using the statistical relation that SEM = $\sigma/\sqrt{n}$, where σ is the SD and n is the number of samples. After performing our experiments, we found the SD among the healthy donor $CD4^+$ T cell counts to be ~180 cells/μl, with a mean of 855 cells/μl (Fig. 5A).

The biochip's $CD4^+/CD8^+$ T cell counts were compared to the gold-standard flow cytometry obtained from Carle Foundation Hospital, Urbana, IL. Eighteen healthy and 32 HIV-infected blood samples (10-μl volume) were evaluated using the electrical differential counting technique. The blood samples were used within 24 hours of acquisition. Infected samples were selected randomly from HIV-infected patients at the Champaign Urbana Public Health District (CUPHD) as they came regularly for measurement of blood cell counts. The patients were asked to participate in the study by the CUPHD caseworkers. If they consented, their blood samples were used in our devices for counting of the target cells. We collected individual samples from one to two HIV-infected patients each day. The patients were not informed of the outcome of the diagnostic results from our device or from the flow cytometry controls, as per the University of Illinois at Urbana-Champaign (UIUC) Institutional Review Board (IRB) protocol. The samples were taken anonymously, such that the authors had no knowledge of the donor's identity, age, gender, or ethnicity. Assessment of the outcomes was blinded as the control counts from flow cytometry were obtained after the biochip experiments were completed. Repeats were performed for both $CD4^+$ and $CD8^+$ T cell counts, and the %CV was calculated from the data in fig. S8.

Blood sample acquisition

The patient blood samples were obtained from the CUPHD according to the UIUC IRB protocol. Blood samples were obtained from volunteers using an informed consent process and monetary compensation approved by the UIUC IRB. Blood was collected via venipuncture in EDTA-coated BD Vacutainers (BD Biosciences), and kept on a rotisserie at room temperature until experiments were performed. Healthy blood donors were recruited among UIUC students with reasonable monetary compensation via another approved UIUC IRB protocol.

Chemicals and reagents

Purified mouse antibody to human CD4 (clone 13B8.2; IM0398, Beckman Coulter Inc.) and purified mouse antibody to human CD8 (clone 3B5; MHCD0800, Life Technologies) were used to capture CD4 and CD8 T cells from the blood. Alexa Fluor 488–conjugated mouse antibody to human CD4 (MHCD0420, Invitrogen), phycoerythrin-Cy7–conjugated mouse antibody to human CD45 (25-0459-42, eBioscience), and peridinin chlorophyll protein–Cy5.5–conjugated mouse antibody to human CD3 (45-0037-42, eBioscience) were used in the capture efficiency experiments.

Microfluidic biochip fabrication and design

Two different chips were used for CD4 and CD8 counting. Figure S1 illustrates the fabrication methods used to create the differential counter chip, which is composed of an electrode layer and a multilevel fluidic layer (Supplementary Methods). The experimental setup is shown in Fig. 1D and also described in Supplementary Methods. The single-capture chamber from our previous work (*24*) was split into eight parallel 2-mm-wide chambers of equal height to effectively create a larger chamber that would have similar wall shear stresses at higher total flow rates to ensure total test times of less than 15 min.

Gating strategy for electrical counting of cells

We used a gating strategy similar to standard flow cytometry methods to quantify the captured lymphocytes. Figure 4F shows a typical example of gating, which is always performed on the low-frequency impedance versus opacity (high-frequency impedance/low-frequency impedance) plots. The distribution on the left (Fig. 4F, red box) represents the lymphocytes during the entrance or exit counts. This red gate representing lymphocytes was drawn between two minimum density values (one between debris and the lymphocyte population, and the other between the lymphocyte and granulocyte/monocyte populations). The number of captured lymphocytes, that is, the target $CD4^+$ T cells, was calculated by subtracting these gated distributions of the exit count from the entrance count. A similar gating strategy could be used to find the difference between entrance and exit counts for the granulocyte/monocyte population (Fig. 6F, rightmost gate) and total leukocytes.

$CD4^+/CD8^+$ T lymphocyte count comparison

The biochip's $CD4^+/CD8^+$ T cell counts were compared to the gold-standard flow cytometry. Whole-blood samples (10 μl) were evaluated using the electrical differential counting technique with on-chip erythrocyte lysis and quenching. Control counts were provided by the Carle Foundation Hospital staff, using a Beckman Coulter FC-500 flow cytometer and the gating strategy described in the equipment operating manual. Whole-blood samples were first incubated with a cocktail of fluorophores to label CD45, CD3, CD4, and CD8 with distinct colors before lysing the erythrocytes and subsequent flow analysis. During post-processing, an initial round of gating was used to isolate the lymphocytes, which are distinguishable from other leukocytes by their bright CD45 levels and low side-scattering characteristics. Using the initial gate, Carle Foundation Hospital staff obtained $CD4^+$ (or $CD8^+$) T lymphocytes by plotting CD3 intensity against CD4 (or CD8) intensity and selecting the $CD3^+CD4^+$ (or $CD3^+CD8^+$) population.

Capture efficiency procedure

Figure S4, A and B, shows the flow cytometry data where total lymphocytes were gated on the basis of their unique side scattering versus CD45 fluorescence intensities, then further gated into different lymphocyte subpopulations. Populations of interest included $CD4^+$ T lymphocytes ($CD3^+CD4^+$, upper right quadrant), T lymphocytes ($CD3^+$, upper two quadrants), and all lymphocytes (all quadrants) (fig. S4B). The fraction of $CD4^+$ lymphocytes was calculated on the basis of the number of upper right quadrant events divided by the events in all quadrants (see equations in Supplementary Methods).

Capture chamber modification for $CD4^+/CD8^+$ T lymphocyte capture

Selective capture of $CD4^+$ or $CD8^+$ T lymphocytes from leukocytes was attained by coating the capture chamber region via simple adsorption with CD4 or CD8 antibody before electrical differential experiments. To obtain CD4 and CD8 counts from one patient, two chips were used simultaneously—one with a capture chamber modified with CD4 antibody, and the other modified with CD8 antibody. Specifically, purified mouse antibody to human CD4 (clone 13B8.2; IM0398, Beckman Coulter Inc.) or purified mouse antibody to human CD8 (clone 3B5; MHCD0800, Life Technologies) was diluted [8 μl antibody + 120 μl PBS (pH 7.4)] and then injected into the capture chambers. The solution was then incubated for 30 min before a second infusion and subsequent incubation period of at least 30 min. The chips were either used immediately after the final incubation period or stored in a 4°C refrigerator for experiments that would be performed on the same day as antibody coating. The antibody solution was washed off with PBS (pH 7.4) immediately before the counting experiments.

Statistical analysis

Bland-Altman analysis was used to measure the agreement between the two cell-counting methods used here: chip and flow cytometry. The Bland-Altman plot was obtained by plotting the difference of the two methods' counts (chip count – flow cytometry count) with the mean of the two methods' counts (average of chip count and flow cytometry control count for every blood sample). It generated a bias value, which indicated a systematic difference between the counts and was calculated by taking the mean difference of the counts. The limits of agreements were calculated as 1.96 × SD of the difference. Two-tailed *P* values were also calculated.

The Pearson coefficient represented the linear relationship between the two methods from chip counts and flow cytometry control counts. Its value ranges from [−1, 1], with 1 representing the perfect correlation of the two methods. Coefficient of determination was also calculated to measure the correlation between the two techniques. A significance level $\alpha = 0.05$ was obtained. $P < 0.0001$ rejected the null hypothesis that there exists no correlation between chip and control counts. Statistical analyses were performed by XLSTAT (data analysis software for Microsoft Excel).

SUPPLEMENTARY MATERIALS

www.sciencetranslationalmedicine.org/cgi/content/full/5/214/214ra170/DC1
Methods
Fig. S1. Microfabrication processes for creating the biochip electrode and fluidic layers.
Fig. S2. Quenching reagent selection and its optimization.
Fig. S3. Process flow graph for the capture efficiency analysis procedure.
Fig. S4. Capture efficiency analysis methodology.
Fig. S5. 3D shear stress simulations along the posts of the capture chamber.
Fig. S6. Capture purity of cells captured with CD4 and CD8 antibodies.
Fig. S7. Comparison of hematocrit, % cell count error, and flow control T cell count for healthy and infected blood donors.
Fig. S8. Repeatability of CD4 and CD8 T cell counts.
Table S1. Time exposure of the lysing and quenching buffers in single- and dual-counter designs at different flow rates.
Table S2. $CD4^+$ and $CD8^+$ T cells obtained from the Carle Hospital flow cytometer and measured from our biochip.
Table S3. Comparison of different CD4 T cell enumeration technologies.
Movie S1. On-chip erythrocyte lysing.
Movie S2. CD4 T cells attaching to the posts via interactions with the CD4 antibodies in the capture chamber.
Movie S3. Another view of CD4 T cells attaching to the posts via interactions with the CD4 antibodies in the capture chamber.
Reference (*36*)

REFERENCES AND NOTES

1. World Health Organization, *Global HIV/AIDS Response: Epidemic Update and Health Sector Progress Towards Universal Access* (World Health Organization, Geneva, 2011).
2. S. Pahwa, J. S. Read, W. Yin, Y. Matthews, W. Shearer, C. Diaz, K. Rich, H. Mendez, B. Thompson, $CD4^+/CD8^+$ T cell ratio for diagnosis of HIV-1 infection in infants: Women and infants transmission study. *Pediatrics* **122**, 331–339 (2008).
3. J. H. Wang, C. H. Wang, C. C. Lin, H. Y. Lei, G. B. Lee, An integrated microfluidic system for counting of $CD4^+/CD8^+$ T lymphocyte. *Microfluid. Nanofluid.* **10**, 531–541 (2011).
4. J. T. Gohring, X. Fan, Label free detection of $CD4^+$ and $CD8^+$ T lymphocytes with the optofluidic ring resonator biosensor. *Sensors* **10**, 5798–5808 (2010).
5. F. M. de Souza, Modeling of the dynamics of HIV-1 and CD4 and CD8 lymphocytes. *IEEE Eng. Med. Biol.* **18**, 21–24 (1999).
6. X. Cheng, A. Gupta, C. Chen, R. G. Tompkins, W. Rodriguez, M. Toner, Enhancing the performance of a point-of-care $CD4^+$ T-cell counting microchip through monocyte depletion for HIV/AIDS diagnostics. *Lab Chip* **9**, 1357–1364 (2009).
7. J. V. Jokerst, J. W. Jacobson, B. D. Bhagwandin, P. N. Floriano, N. Christodoulides, J. T. McDevitt, Programmable nano-bio-chip sensors: Analytical meets clinical. *Anal. Chem.* **82**, 1571–1579 (2010).
8. M. Beck, S. Brockhuis, N. van der Velde, C. Breukers, J. Greve, L. W. Terstappen, On-chip sample preparation by controlled release of antibodies for simple CD4 counting. *Lab Chip* **12**, 167–173 (2012).
9. Y. C. Manabe, Y. Wang, A. Elbireer, B. Auerbach, B. Castelnuovo, Evaluation of portable point-of-care CD4 counter with high sensitivity for detecting patients eligible for antiretroviral therapy. *PLOS One* **7**, e34319 (2012).
10. B. Wang, A. L. Weldon, P. Kumnorkaew, B. Xu, J. F. Gilchrist, X. Cheng, Effect of surface nanotopography on immunoaffinity cell capture in microfluidic devices. *Langmuir* **27**, 11229–11237 (2011).
11. S. J. Moon, H. O. Keles, A. Ozcan, A. Khademhosseini, E. Hæggstrom, D. Kuritzkes, U. Demirci, Integrating microfluidics and lensless imaging for point-of-care testing. *Biosens. Bioelectron.* **24**, 3208–3214 (2009).
12. P. Kiesel, M. Beck, N. Johnson, Monitoring CD4 in whole blood with an opto-fluidic detector based on spatially modulated fluorescence emission. *Cytometry A* **79A**, 317–324 (2011).
13. D. S. Boyle, K. R. Hawkins, M. S. Steele, M. Singhal, X. Cheng, Emerging technologies for point-of-care CD4 T-lymphocyte counting. *Trends Biotechnol.* **30**, 45–54 (2012).
14. R. Zachariah, S. D. Reid, P. Chaillet, M. Massaquoi, E. J. Schouten, A. D. Harries, Viewpoint: Why do we need a point-of-care CD4 test for low-income countries? *Trop. Med. Int. Health* **16**, 37–41 (2011).
15. J. Bocsi, D. Lenz, A. Mittag, V. S. Varga, B. Molnar, Z. Tulassay, U. Sack, A. Tárnok, Automated four-color analysis of leukocytes by scanning fluorescence microscopy using quantum dots. *Cytometry A* **69**, 131–134 (2006).
16. K. Cheung, S. Gawad, P. Renaud, Impedance spectroscopy flow cytometry: On-chip label-free cell differentiation. *Cytometry A* **65A**, 124–132 (2005).
17. C. Kuttel, E. Nascimento, N. Demierre, T. Silva, T. Braschler, P. Renaud, A. G. Oliva, Label-free detection of *Babesia bovis* infected red blood cells using impedance spectroscopy on a microfabricated flow cytometer. *Acta Trop.* **102**, 63–68 (2007).
18. A. Pierzchalski, M. Hebeisen, A. Mittag, M. D. Berardino, A. Tarnok, Label-free single cell analysis with a chip-based impedance flow cytometer. *Proc. SPIE* **7568**, 75681B (2010).
19. G. Schade-Kampmann, A. Huwiler, M. Hebeisen, T. Hessler, M. Di Berardino, On-chip non-invasive and label-free cell discrimination by impedance spectroscopy. *Cell Prolif.* **41**, 830–840 (2008).
20. K. C. Cheung, M. Di Berardino, G. Schade-Kampmann, M. Hebeisen, A. Pierzchalski, J. Bocsi, A. Mittag, A. Tárnok, Microfluidic impedance-based flow cytometry. *Cytometry A* **77A**, 648–666 (2010).
21. G. Benazzi, D. Holmes, T. Sun, M. C. Mowlem, H. Morgan, Discrimination and analysis of phytoplankton using a microfluidic cytometer. *IET Nanobiotechnol.* **1**, 94–101 (2007).
22. C. van Berkel, J. D. Gwyer, S. Deane, N. Green, J. Holloway, V. Hollis, H. Morgan, Integrated systems for rapid point of care (PoC) blood cell analysis. *Lab Chip* **11**, 1249–1255 (2011).
23. D. Holmes, H. Morgan, Single cell impedance cytometry for identification and counting of CD4 T-cells in human blood using impedance labels. *Anal. Chem.* **82**, 1455–1461 (2010).
24. N. N. Watkins, S. Sridhar, X. Cheng, G. D. Chen, M. Toner, W. Rodriguez, R. Bashir, A microfabricated electrical differential counter for the selective enumeration of $CD4^+$ T lymphocytes. *Lab Chip* **11**, 1437–1447 (2011).
25. W. H. Coulter, Means for counting particles suspended in a fluid, U.S. Patent 2656508 (1953).
26. D. Holmes, D. Pettigrew, C. H. Reccius, J. D. Gwyer, C. van Berkel, J. Holloway, D. E. Davies, H. Morgan, Leukocyte analysis and differentiation using high speed microfluidic single cell impedance cytometry. *Lab Chip* **9**, 2881–2889 (2009).
27. X. Cheng, Y. Liu, D. Irimia, U. Demirci, L. Yang, L. Zamir, W. R. Rodriguez, M. Toner, R. Bashir, Cell detection and counting through cell lysate impedance spectroscopy in microfluidic devices. *Lab Chip* **7**, 746–755 (2007).
28. R. A. Hoffman, W. B. Britt, Flow-system measurement of cell impedance properties. *J. Histochem. Cytochem.* **27**, 234–240 (1979).
29. S. Gawad, L. Schild, P. Renaud, Micromachined impedance spectroscopy flow cytometer for cell analysis and particle sizing. *Lab Chip* **1**, 76–82 (2001).
30. M. C. Jacob, M. Favre, J. C. Bensa, Membrane cell permeabilization with saponin and multiparametric analysis by flow cytometry. *Cytometry* **12**, 550–558 (1991).
31. H. P. Schwan, Electrical properties of blood and its constituents: Alternating current spectroscopy. *Blut* **46**, 185–197 (1983).
32. H. Morgan, T. Sun, D. Holmes, S. Gawad, N. G. Green, Single cell dielectric spectroscopy. *J. Phys. D: Appl. Phys.* **40**, 61–70 (2007).
33. S. H. Zuckerman, S. K. Ackerman, S. D. Douglas, Long-term human peripheral blood monocyte cultures: Establishment, metabolism and morphology of primary human monocyte-macrophage cell cultures. *Immunology* **38**, 401–411 (1979).
34. C. A. Lundquist, M. Tobiume, J. Zhou, D. Unutmaz, C. Aiken, Nef-mediated downregulation of CD4 enhances human immunodeficiency virus type 1 replication in primary T lymphocytes. *J. Virol.* **76**, 94625–94633 (2002).
35. I. Jani, N. Sitoe, P. Chongo, E. Alfai, J. Quevedo, O. Tobaiwa, J. Lehe, T. Peter, Accurate CD4 T-cell enumeration and antiretroviral drug toxicity monitoring in primary healthcare clinics using point-of-care testing. *AIDS* **25**, 807–812 (2011).
36. K. Srithanaviboonchai, K. Rungruengthanakit, P. Nouanthong, S. Pata, T. Sirisanthana, W. Kasinrerk, Novel low-cost assay for the monitoring of CD4 counts in HIV-infected individuals. *J. Acquir. Immune Defic. Syndr.* **47**, 135–139 (2008).

Acknowledgments: We thank N. Won, A. Czapar, and C. Edwards for help with data analysis and PDMS device fabrication, and X. Cheng (Lehigh University), M. Toner (Massachusetts General Hospital), and R. Suva, J. Roche, F. Farber, and M. Fernandez Suarez (Daktari Diagnostics Inc.) for helpful discussions. We acknowledge D. Heath, P. Woo, and B. Stillwell of Carle Foundation Hospital for their help in obtaining samples from student donors. We thank S. Grove and K. Dyer of Carle Foundation Hospital and M. Helms of UIUC for their help in organizing and obtaining control cell counts. We thank G. Dunn, P. Shonkwiler, and C. Crause at the CUPHD for assistance in providing HIV^+ patient samples. **Funding:** R.B. acknowledges the support of the NSF Nanoscale Science and Engineering Center at Ohio State University (grant number EEC-0914790) and funding from the University of Illinois, Urbana-Champaign. We also acknowledge funding from NSF IUCRC Center for Agricultural, Biomedical, and Pharmaceutical Nanotechnology at UIUC. N.N.W. was supported in part by a Department of Homeland Security fellowship. G.D. was supported by the Roy J. Carver Fellowship and the Illinois Distinguished Fellowship. **Author contributions:** U.H. performed CD4 and CD8 cell counting experiments with healthy and patient samples. He also performed flow cytometry for capture efficiency experiments and analyzed data and calculated statistics. N.N.W. did lysing and quenching time optimization with statistical calculations, did device design and fabrication, acquired healthy participant samples, and initiated procurement and testing of healthy and infected participant samples. G.D. acquired patient samples, performed flow cytometry, and

fabricated the device. H.N. fabricated the device. W.R. and R.B. conceived the idea. N.N.W., U.H., and R.B. designed the study and wrote the paper. A.V. arranged patient samples from CUPHD and assisted in data analysis. **Competing interests:** W.R. and R.B. have financial interests in Daktari Diagnostics Inc. A joint provisional patent has been filed among UIUC, Daktari Diagnostics, Massachusetts General Hospital, and Massachusetts Institute of Technology. **Data and materials availability:** The devices and materials mentioned in this paper will be available on any reasonable request upon completion of a materials transfer agreement between requestor and university.

Submitted 24 June 2013
Accepted 12 November 2013
Published 4 December 2013
10.1126/scitranslmed.3006870

Citation: N. N. Watkins, U. Hassan, G. Damhorst, H. Ni, A. Vaid, W. Rodriguez, R. Bashir, Microfluidic $CD4^+$ and $CD8^+$ T lymphocyte counters for point-of-care HIV diagnostics using whole blood. *Sci. Transl. Med.* **5**, 214ra170 (2013).